Trop2 is a driver of metastatic prostate cancer with neuroendocrine phenotype via PARP1

En-Chi Hsu[a,b], Meghan A. Rice[a,b], Abel Bermudez[a,b], Fernando Jose Garcia Marques[a,b], Merve Aslan[a,b], Shiqin Liu[a,b], Ali Ghoochani[a,b], Chiyuan Amy Zhang[c], Yun-Sheng Chen[a,b], Aimen Zlitni[a,b], Sahil Kumar[d], Rosalie Nolley[c], Frezghi Habte[a,b], Michelle Shen[a,b], Kashyap Koul[a,b], Donna M. Peehl[e], Amina Zoubeidi[d], Sanjiv S. Gambhir[a,b,f,g,h,i], Christian A. Kunder[j], Sharon J. Pitteri[a,b,f], James D. Brooks[b,c,f], and Tanya Stoyanova[a,b,f,1]

[a]Department of Radiology, Stanford University, Stanford, CA 94304; [b]Canary Center at Stanford for Cancer Early Detection, Stanford University, Stanford, CA 94304; [c]Department of Urology, Stanford University, Stanford, CA 94304; [d]Department of Urologic Sciences, University of British Columbia, Vancouver, BC V6H 3Z6, Canada; [e]Department of Radiology and Biomedical Imaging, University of California, San Francisco, CA 94143; [f]Bio-X Program, Stanford University, Stanford, CA 94305; [g]Department of Bioengineering, Stanford University, Stanford, CA 94305; [h]Department of Materials Science & Engineering, Stanford University, Stanford, CA 94305; [i]Molecular Imaging Program at Stanford, Stanford University, Stanford, CA 94305; and [j]Department of Pathology, Stanford University, Stanford, CA 94304

Edited by Myles Brown, Dana-Farber/Brigham and Women's Cancer Center, Boston, MA, and approved December 18, 2019 (received for review March 29, 2019)

Resistance to androgen deprivation therapy, or castration-resistant prostate cancer (CRPC), is often accompanied by metastasis and is currently the ultimate cause of prostate cancer-associated deaths in men. Recently, secondary hormonal therapies have led to an increase of neuroendocrine prostate cancer (NEPC), a highly aggressive variant of CRPC. Here, we identify that high levels of cell surface receptor Trop2 are predictive of recurrence of localized prostate cancer. Moreover, Trop2 is significantly elevated in CRPC and NEPC, drives prostate cancer growth, and induces neuroendocrine phenotype. Overexpression of Trop2 induces tumor growth and metastasis while loss of Trop2 suppresses these abilities in vivo. Trop2-driven NEPC displays a significant up-regulation of PARP1, and PARP inhibitors significantly delay tumor growth and metastatic colonization and reverse neuroendocrine features in Trop2-driven NEPC. Our findings establish Trop2 as a driver and therapeutic target for metastatic prostate cancer with neuroendocrine phenotype and suggest that high Trop2 levels could identify cancers that are sensitive to Trop2-targeting therapies and PARP1 inhibition.

prostate | cancer | NEPC | Trop2

Approximately 31,620 men are projected to die from prostate cancer in the United States in 2019, making it the second leading cause of male cancer death (1). Advanced prostate cancer, whether present at the time of diagnosis or arising after treatment of localized disease, responds to androgen deprivation but invariably fails and recurs as castration-resistant prostate cancer (CRPC), which is the main cause of prostate cancer-associated mortality (2, 3). Heavily treated tumors, particularly those treated with secondary hormone therapies, frequently acquire a neuroendocrine phenotype (neuroendocrine prostate cancer [NEPC]), which currently accounts for 10 to 20% of CRPC (4, 5). Although rare, de novo NEPC is also observed in less than 2% of prostate cancer at the time of diagnosis (4). NEPC is commonly characterized by expression of neuroendocrine markers, an aggressive clinical course, and down-regulation or loss of androgen receptor (AR) that diminishes responsiveness to androgen deprivation therapies, making it the most lethal and currently incurable subset of prostate cancer (6–9).

Tumor-associated calcium signal transducer 2 (Tacstd2, Trop2, TROP2) is a cell surface glycoprotein that has emerged as a promising therapeutic target due to its overexpression in multiple epithelial cancers (10, 11). Sacituzumab govitecan (IMMU-132), an anti-Trop2 antibody conjugated with SN-38, a cytotoxic agent that targets DNA replication, has shown therapeutic activity in several malignances, including triple negative breast cancer, advanced non-small cell lung cancer, and metastatic platinum-resistant urothelial carcinoma (10, 12–14).

In the prostate, Trop2 is an important regulator of prostate stem cell self-renewal (15). Murine prostate basal cells with high levels of Trop2 can regenerate prostatic tubules, and Trop2-positive epithelial cells are enriched after androgen ablation (16), suggesting that Trop2 has roles in cell survival after androgen ablation and lineage plasticity during the regeneration of prostate-like structures after androgen repletion. Trop2 is activated through proteolytic cleavages (15, 17) and is involved in prostate cancer metastasis through β1 integrin and FAK signaling (18, 19).

Herein, we demonstrate that an elevated level of Trop2 is prognostic for biochemical recurrence and even higher level of Trop2 is found in metastatic CRPC and NEPC. Deletion of the TROP2 gene significantly slows cell growth and decreases migration, invasion, and metastatic colonization of prostate cancer cells while overexpression of Trop2 increases growth, invasion, and metastasis. Overexpression of Trop2 leads to a significant decrease in luminal markers, such as androgen receptor (AR), and Trop2 enhances tumor growth while also inducing lineage plasticity, neuroendocrine features, and metastasis in vivo. Trop2-expressing prostate cancer xenografts are resistant to androgen ablation and express high levels of PARP1. PARP1 inhibitors decrease cell proliferation and neuroendocrine markers and suppress the growth and metastasis of Trop2-driven tumors. Our

Significance

NEPC is a highly aggressive subtype of prostate cancer that is increasing in incidence, likely due to use of new secondary androgen deprivation therapies. Here, we demonstrate that Trop2 is significantly elevated in CRPC and NEPC and represents a driver of metastatic NEPC. Trop2 overexpression increases tumor growth, drives metastasis and neuroendocrine phenotype, and significantly increases PARP1 levels. Inhibition of PARP1 in Trop2-driven NEPC significantly decreases neuroendocrine features, tumor growth, and metastatic colonization in vivo, suggesting that PARP1 inhibitors may represent a promising therapeutic strategy for metastatic prostate cancer expressing high levels of Trop2.

Author contributions: D.M.P., A. Zoubeidi, S.S.G., S.J.P., J.D.B., and T.S. designed research; E.-C.H., M.A.R., A.B., F.J.G.M., M.A., S.L., A.G., C.A.Z., Y.-S.C., A. Zlitni, S.K., R.N., F.H., M.S., K.K., C.A.K., S.J.P., and T.S. performed research; E.-C.H., D.M.P., A. Zoubeidi, and T.S. contributed new reagents/analytic tools; E.-C.H., A.B., F.J.G.M., C.A.Z., Y.-S.C., A. Zlitni, S.K., R.N., D.M.P., A. Zoubeidi, C.A.K., S.J.P., J.D.B., and T.S. analyzed data; and E.-C.H., M.A.R., D.M.P., A. Zoubeidi, S.S.G., C.A.K., S.J.P., J.D.B., and T.S. wrote the paper.

The authors declare no competing interest.

This article is a PNAS Direct Submission.

[1]To whom correspondence may be addressed. Email: stanya@stanford.edu.

This article contains supporting information online at https://www.pnas.org/lookup/suppl/doi:10.1073/pnas.1905384117/-/DCSupplemental.

First published January 13, 2020.

results demonstrate that Trop2 plays a functional role in driving neuroendocrine phenotype and provide strong functional evidence that targeting Trop2 and Trop2 signaling cascade through PARP1 inhibition may represent a novel rational therapeutic strategy for metastatic prostate cancer with high levels of Trop2.

Results

High Expression of Trop2 Is Prognostic for Prostate Cancer Recurrence. Given the important role of Trop2 in prostate stem cell biology (15), we assessed Trop2 protein levels of benign human prostate tissues ($n = 26$) and localized prostate cancer ($n = 79$) by immunohistochemistry (IHC) (Fig. 1*A* and *SI Appendix*, Fig. S1*A*) and found relatively higher expression levels in prostate cancer compared to benign prostate tissues (Fig. 1*A*). Consistent with previous reports, Trop2 expression was restricted to basal cells in the normal prostate (*SI Appendix*, Fig. S1*B*) (16). We further evaluated Trop2 levels in the resected prostates of a cohort of 234 prostate cancer patients who underwent radical prostatectomy with median 9-y follow-up in which 58 patients displayed biochemical recurrence (Fig. 1 *B* and *C*). High expression of Trop2 was associated with biochemical recurrence in a univariable model ($P = 0.01$) and independently associated with recurrence in a multivariable model ($P < 0.05$) that included preoperative serum prostate-specific antigen (PSA) levels, a pathological stage, and pathological Gleason score. Interestingly, most patients with concurrent lymph node metastases or who later developed bone metastasis showed high expression of Trop2 in their prostatectomy specimens ($P = 0.02$) (Fig. 1*D*). These results demonstrate that high levels of Trop2 correlate with unfavorable outcomes in prostate cancer.

Trop2 Regulates Prostate Cancer Cell and Tumor Growth In Vitro and In Vivo. To determine the functional role of Trop2 in prostate tumorigenesis, we first assessed the levels of Trop2 in a panel of prostate cell lines (*SI Appendix*, Fig. S2*A*). We then generated stable lines of DU145, a prostate cancer cell line that expresses Trop2, by deleting the TROP2 gene using CRISPR/Cas9n (DU145-TROP2-KO) technology (*SI Appendix*, Fig. S2 *B* and *C*). A DU145 cell line with overexpression of red fluorescent protein (RFP) (DU145-RFP) or RFP and Trop2 was created by lentiviral transduction (DU145-Trop2-OV) (Fig. 2*A*). Likewise, we generated stable lines of the prostate cancer cell lines with low/no detectable Trop2 at baseline, such as LNCaP, PC-3, and VCaP cells that overexpress Trop2 and RFP (LNCaP-Trop2-OV, PC-3-Trop2-OV, and VCaP-Trop2-OV, respectively). Cell proliferation was evaluated by cell counts in DU145 and LNCaP over 6 d (Fig. 2 *B* and *C*). Loss of TROP2 resulted in a significant decrease in cell proliferation while up-regulation of Trop2 significantly enhanced cell proliferation (Fig. 2 *B* and *C*). In clonogenic and tumorsphere assays, loss of TROP2 expression in DU145 led to a significant decrease in colony and tumorsphere formation while overexpression significantly enhanced colony and tumorsphere formation (Fig. 2*D* and *SI Appendix*, Fig. S2*D*). LNCaP cells normally do not form colonies, but overexpression of Trop2 significantly enhanced colony formation and tumorsphere growth in LNCaP cells (Fig. 2*E*). Knockdown of TROP2 in LNCaP-Trop2-OV cells significantly reduced cell proliferation and colony formation driven by Trop2, further supporting the role of Trop2 in prostate cancer cell growth (*SI Appendix*, Fig. S2 *E*–*G*). Overexpression of Trop2 also significantly increased growth of PC-3 and VCaP cells assessed by colony formation and tumorsphere assays (*SI Appendix*, Fig. S3 *A*–*E*).

We further investigated the functional role of Trop2 in prostate tumorigenesis in vivo. LNCaP-RFP or LNCaP-Trop2-OV cells were implanted subcutaneously (s.c.) into the flanks of immunodeficient NOD SCID gamma mice (NSG). Overexpression of Trop2 resulted in dramatically increased LNCaP tumor growth assessed by tumor volumes and tumor weights (Fig. 2*F*). As expected, LNCaP-Trop2-OV tumors expressed high levels of Trop2 while LNCaP-RFP had no detectable Trop2 determined by IHC (Fig. 2 *F*, *Lower*). Similar results were observed using DU145 prostate cancer cells where overexpression of Trop2 significantly increased tumor burden (Fig. 2*G*). Since DU145 cells normally express Trop2, we tested whether gene deletion of TROP2 (DU145-TROP2-KO) affected tumor growth (Fig. 2*H* and *SI Appendix*, Fig. S4). Compared to parental DU145 cells or control DU145 cell lines, three independent clones of DU145-TROP2-KO cells displayed a significant decrease in tumor growth (Fig. 2*H* and *SI Appendix*, Fig. S4 *A* and *B*), implicating Trop2 as a key regulator of prostate cancer growth in vivo.

Trop2 Regulates Prostate Cancer Cell Migration and Invasion In Vitro. Migration of cancer cells and invasion of surrounding tissues are hallmarks of cancer progression. We next evaluated the role of Trop2 in prostate cancer invasion and migration in vitro. In Boyden chamber assays, DU145 cells lacking TROP2 demonstrated significantly decreased migration while cells overexpressing Trop2 exhibited enhanced migration (Fig. 3*A* and *SI Appendix*, Fig. S5*A*). Similarly, wound-healing assays revealed enhanced cell migration

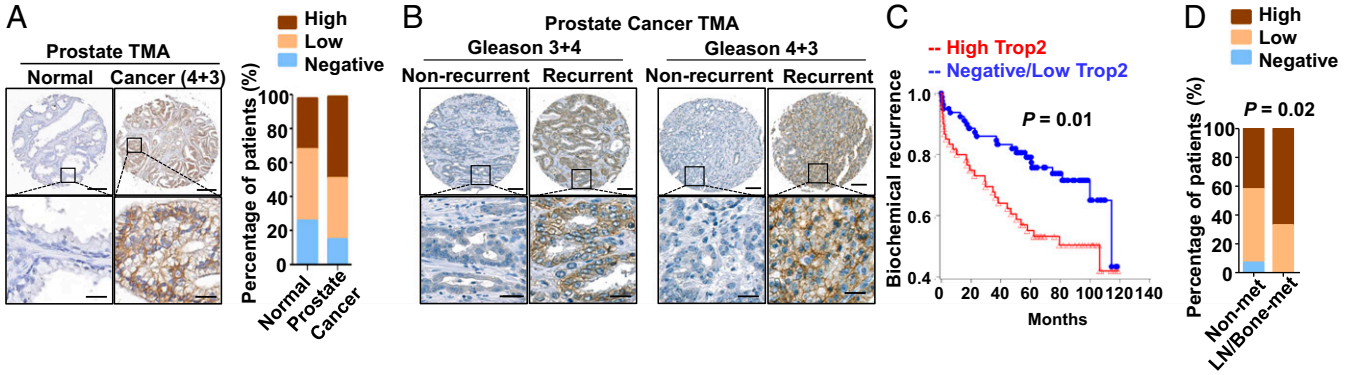

Fig. 1. Trop2 is elevated in prostate cancer and positively associated with biochemical recurrence and metastatic risk. (*A*) IHC staining of Trop2 on tissue microarrays (TMAs) composed of normal prostate ($n = 26$) and prostate cancer Gleason 4+3 ($n = 79$). Trop2 staining intensity was scored from 0 to 3 (0 is negative, 1 is uninterpretable, 2 is weak positive [low], 3 is strong positive [high]). Representative images for negative and high staining are shown. (Scale bars represent 200 and 25 μm, respectively [enlarged images].) Examples for negative, low, and high Trop2 staining are shown in *SI Appendix*, Fig. S1. (*Right*) Represents the distribution of Trop2 intensity scores as a percentage of patient samples. (*B*) Trop2 IHC on independent TMAs with associated clinical and pathological data. Representative images for Trop2 staining of patient samples with different Gleason scores and recurrence status are shown. (Scale bars represent 200 and 25 μm, respectively [enlarged images in *Lower*].) (*C*) Strong staining for Trop2 correlates with prostate cancer recurrence after prostatectomy (recurrent patients, $n = 58$, and nonrecurrent patients, $n = 176$). $P = 0.01$ by log-rank test. (*D*) Strong Trop2 expression correlates with prostate cancer metastasis. Samples from patients with no metastasis (Non-met) ($n = 204$) and patients with metastasis ($n = 18$, including lymph node [LN] [$n = 12$] and bone metastasis [$n = 6$]) were used. The statistical significance of the differences between no metastasis and metastasis proportions was calculated by the normal distribution N(0,1) of the z-score. $P = 0.02$.

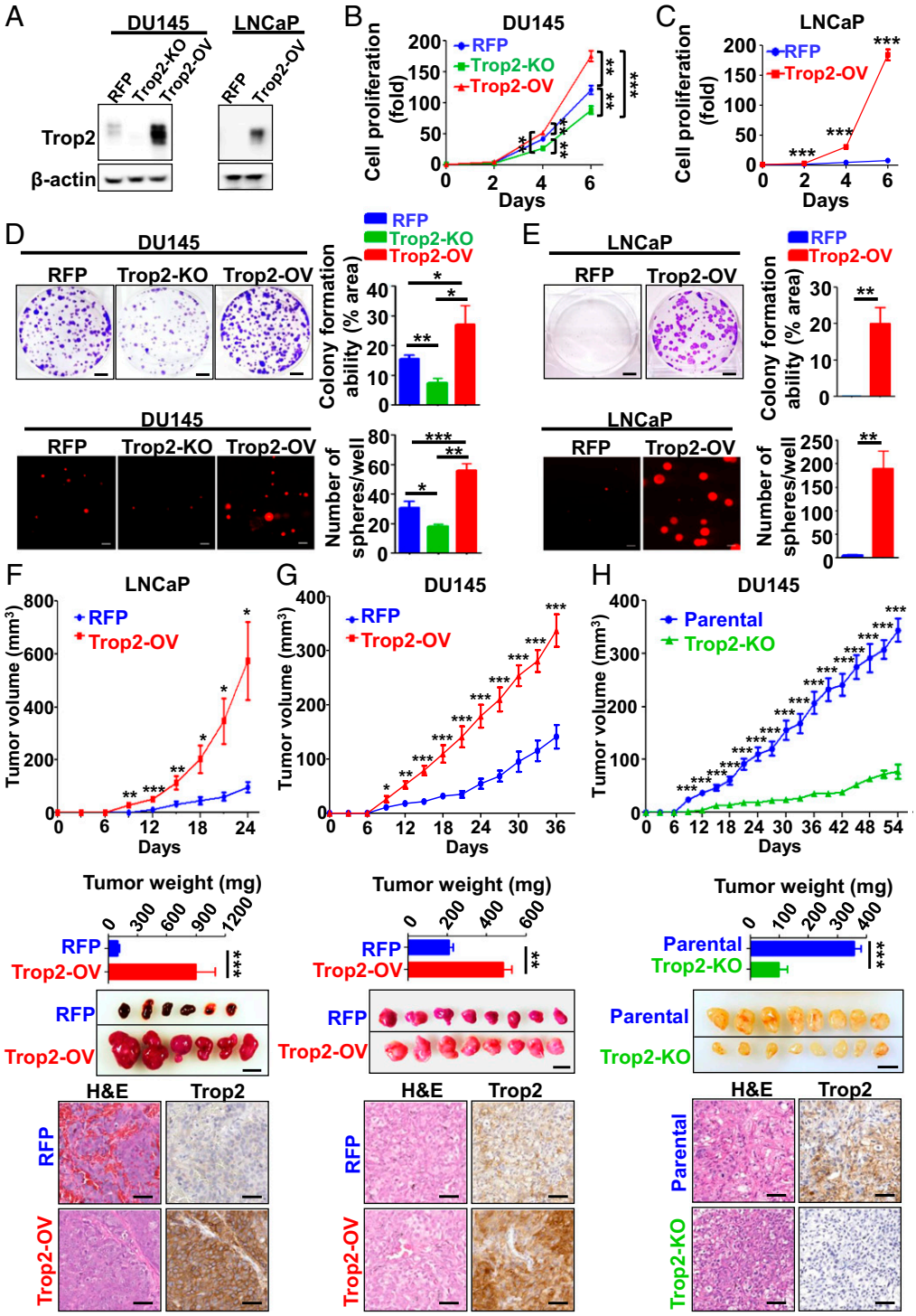

Fig. 2. Trop2 regulates prostate cancer cell proliferation and clonogenic ability in vitro and in vivo. (*A*) Trop2 level was assessed by Western blot in DU145 and LNCaP cells expressing RFP, TROP2 gene deletion (DU145-Trop2-KO), and in cell lines overexpressing Trop2 (DU145-Trop2-OV, LNCaP-Trop2-OV). Trop2 appears as doublets or a smear on Western blot due to glycosylation. (*B*) Cell proliferation graphed as fold-change (compared to the time of plating, day 0) of DU145-RFP, DU145-Trop-KO, or DU145-Trop2-OV cells. (*C*) Cell proliferation graphed as fold-change in cell number of LNCaP-RFP or LNCaP-Trop2-OV cells. (*D*, *Upper*) Colony formation assays of 500 DU145-RFP, DU145-Trop2-KO, and DU145-Trop2-OV cells grown for 9 d and then fixed and stained with crystal violet. The percentage of colony area per well was quantified using ImageJ and is shown in the right graph. (Scale bar, 1 cm.) (*D*, *Lower*) Tumorsphere formation assays for DU145-RFP, DU145-Trop2-KO, and DU145-Trop2-OV cells. The number of tumorspheres per well at day 12 is shown in the *Right Graph*. (Scale bar: 300 μm.) (*E*, *Upper*) Colony formation assays for 500 LNCaP-RFP and LNCaP-Trop2-OV cells. (*E*, *Lower*) Representative images of tumorsphere assays for LNCaP-RFP and LNCaP-Trop2-OV at day 15. (Scale bar: 300 μm.) Number of spheres per well is plotted to the *Right*. All experiments were performed in triplicate. Error bars represent SD. (*F–H*) The s.c. tumor growth of LNCaP-RFP or LNCaP-Trop2-OV ($n = 6$) (*F*), DU145-RFP or DU145-Trop2-OV ($n = 8$) (*G*), and DU145 Parental or DU145-Trop2-KO ($n = 8$) (*H*) tumors, respectively, grown in intact male NSG mice. A total of 1×10^6 cells were injected per tumor. Tumor weights, tumors, hematoxylin/eosin (H&E)-stained tumor sections, and Trop2 IHC of tumor sections are shown below in all panels. In *G* and *H*, tumors were harvested when one of the experiment groups reached 350 mm^3 tumor volume on average. (Scale bar for tumor images: 1 cm scale bar for IHC = 50 μm.) Error bars represent SEM. $^*P < 0.05$, $^{**}P < 0.01$, $^{***}P < 0.005$; n.s., not significant; determined by Student's *t* test (two-tailed) at each time point.

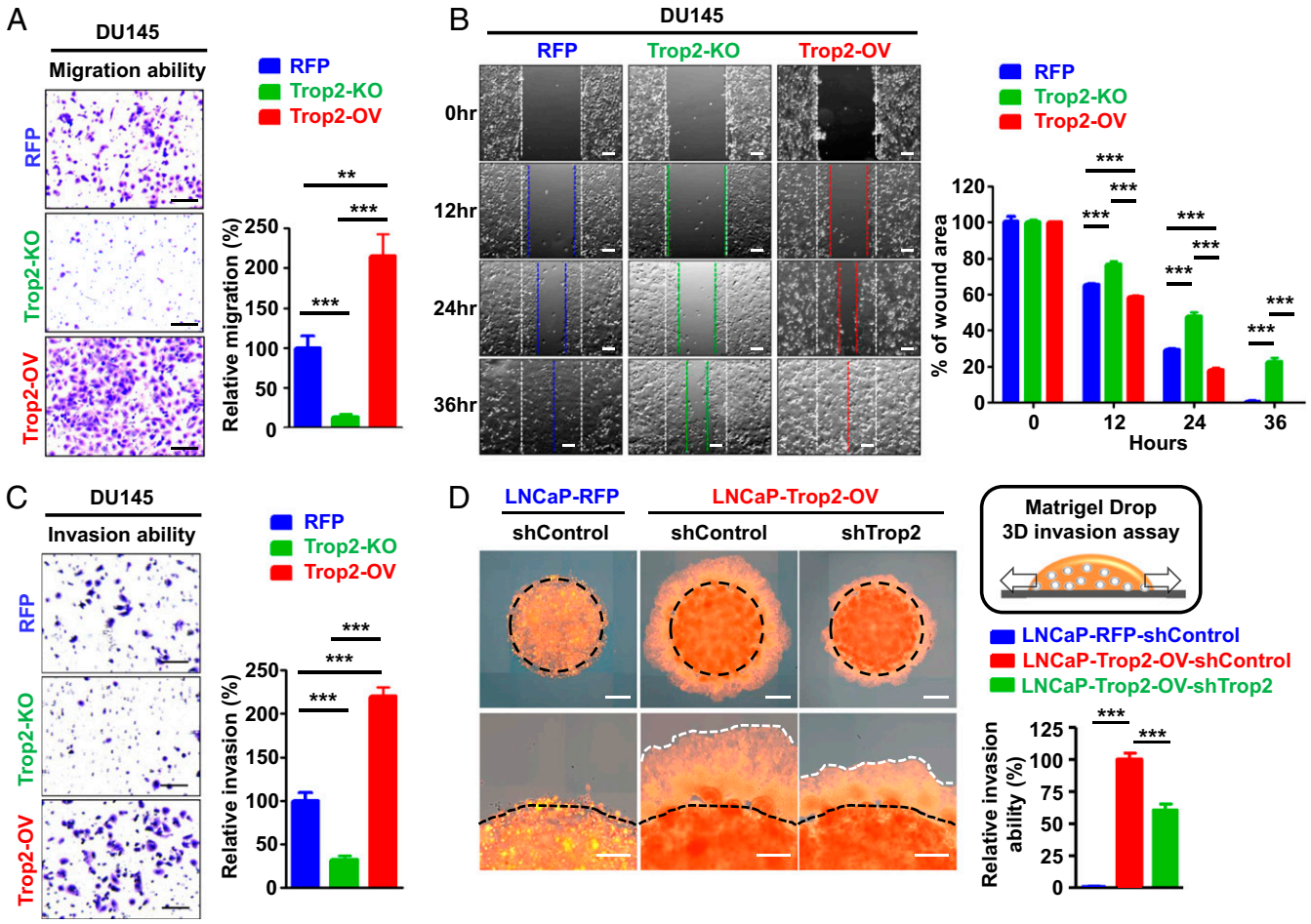

Fig. 3. Trop2 regulates migration and invasion in vitro. (*A*) Transwell chamber assays to assess migration after 20 h incubation of DU145-RFP, DU145-Trop2-KO, and DU145-Trop2-OV cells. Experiments were performed in triplicate, and three images per well were used to quantify stained cells that had migrated. The average number of cells in nine fields (three wells) and percentage of migration were normalized to the DU145-RFP cell counts. One of three independent experiments is shown. (Scale bars: 100 μm.) (*B*) Wound healing assays for DU145- RFP, DU145-Trop2-KO, and DU145-Trop2-OV cells. Experiments were performed in triplicate, and 10 images were acquired per well at 0, 12, 24, and 36 h. The average of the wound area in three wells at 0 h was assigned 100% and used to quantify changes in wound area over time. Representative images are shown. (Scale bar: 100 μm.) (*C*) Boyden chamber assays to assess invasion of DU145-RFP, DU145-Trop2-KO, and DU145-Trop2-OV cells into a Matrigel-coated insert membrane after 20 h. Representative experiment. (Scale bar: 100 μm.) (*D*) Matrigel drop 3D invasion assay using LNCaP-RFP and LNCaP-Trop2-OV cells with control shRNA (shControl) or Trop2 shRNA (shTrop2). Cancer cells (5×10^4) in Matrigel were seeded in a 24-well plate, and drops were imaged at day 0 and day 6 using Celigo imager. The cell migration area outside of the drop was measured. Experiments were performed in triplicate, and the relative invasion ability of cancer cells was normalized to the Trop2-OV group. Orange pseudocolor represents living cells from RFP fluorescent signal of stable clones. (Scale bars: 1 mm and 500 μm [enlarged images].) Error bars represent SD. $^{**}P < 0.01$ and $^{***}P < 0.005$ by Student's *t* test.

with overexpression of Trop2 and significantly decreased migration in the cells lacking TROP2 (Fig. 3*B*). Transwell assays demonstrated that overexpression of Trop2 promoted invasion and loss of TROP2 decreased invasion of DU145 cells (Fig. 3*C*). These findings were confirmed using PC-3-Trop2-OV cells (*SI Appendix*, Fig. S5 *B* and *C*). LNCaP cells normally have little motility when cultured in vitro, and LNCaP-RFP cells grown in a Matrigel drop remain confined within the Matrigel (Fig. 3*D* and *SI Appendix*, Fig. S5*D*). However, LNCaP-Trop2-OV cells invaded through the edge of the Matrigel drop and migrated away from the edge of the drop (Fig. 3*D* and *SI Appendix*, Fig. S5*D*), and knockdown of Trop2 in these cells led to a significant decrease in LNCaP-Trop2-OV migration (Fig. 3*D*). These results support a role of Trop2 in driving an invasive phenotype.

Overexpression of Trop2 Drives Prostate Cancer Colonization and Metastasis While Loss of Trop2 Diminishes Prostate Cancer Colonization to the Bone. To evaluate the effect of Trop2 on prostate cancer metastasis in vivo, we first measured the effect of Trop2 modulation on the ability of prostate cancer cells to home at distant sites assessed by an intracardiac injection model. We used LNCaP-RFP (control cells) and LNCaP-Trop2-OV (LNCaP Trop2 overexpressing cells) transduced with a lentivirus expressing luciferase. Whole body bioluminescence imaging (BLI) and quantification, reflecting homing potential and metastatic burden 21 d after injection, demonstrated that LNCaP-Trop2-OV cells colonized in diverse organs based on RFP signals of harvested tissues (Fig. 4*A* and *SI Appendix*, Fig. S6 *A*, *Left*). Clinically, bone is the most common site of prostate cancer metastasis while liver metastasis correlates with worst overall survival in CRPC patients and is more common in NEPC (20). Bone lesions were identified in the tibias of mice injected with LNCaP-Trop2-OV cells by micro-computed tomography (μCT) (Fig. 4*B*) and by small animal positron-emission tomography (PET)/CT imaging using F18-FDG as a tracer (*SI Appendix*, Fig. S6 *A*, *Right*) while no bone lesions were observed in LNCaP-RFP controls (Fig. 4*B* and *SI Appendix*, Fig. S6*A*). To confirm the imaging findings, tibias were harvested, and RFP signal was measured. Strong RFP signal was detected in the tibias of 30% of the animals injected with LNCaP-Trop2-OV while no signal was detected in the LNCaP-RFP controls (Fig. 4*C*).

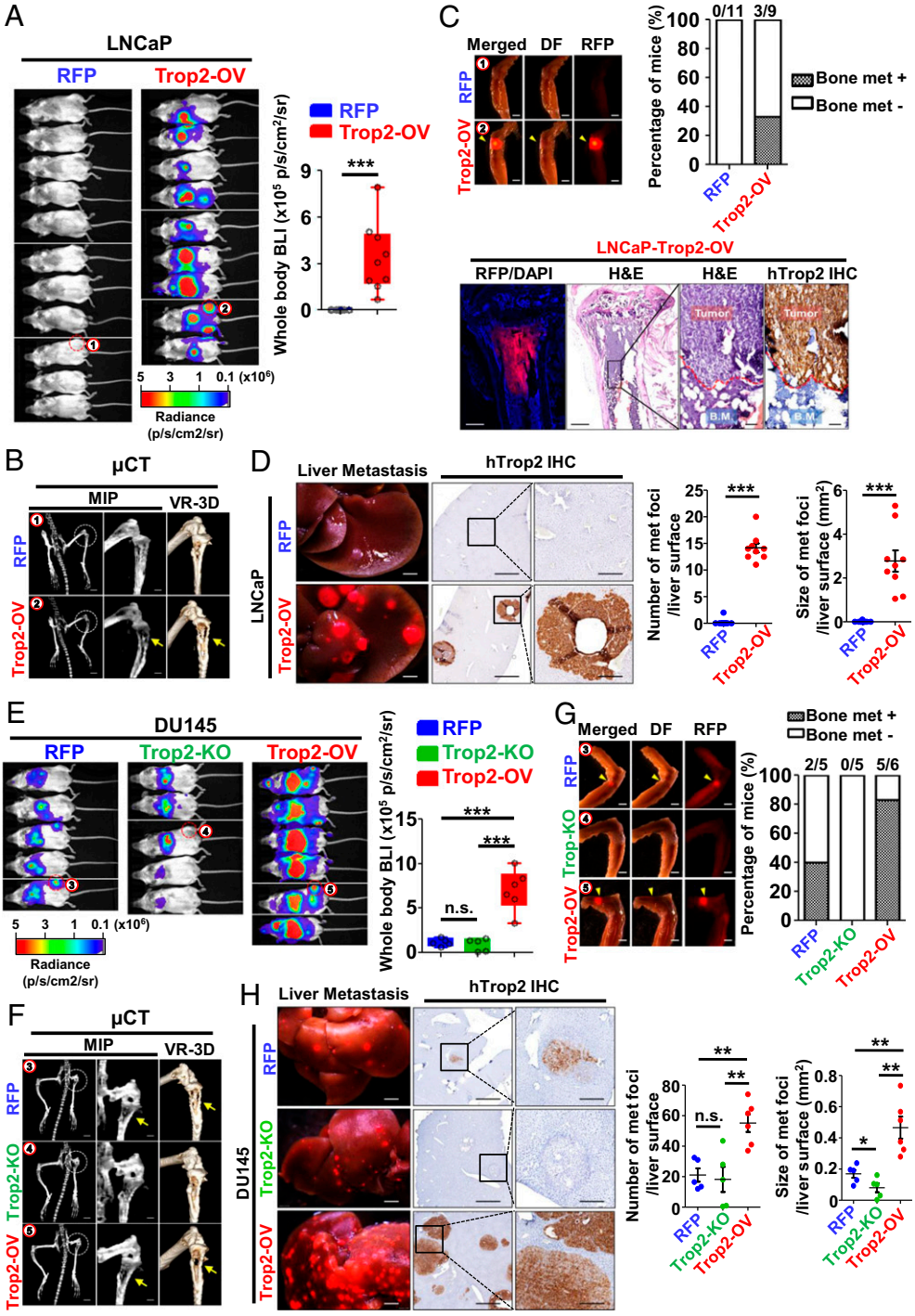

Fig. 4. Trop2 drives bone and liver metastasis in vivo. (*A*) LNCaP-RFP and LNCaP-Trop2-OV cells (1×10^5) expressing luciferase and RFP were injected into the left ventricle of male NSG mice ($n = 11$ and $n = 9$). Whole body bioluminescence intensity (BLI) (photons/second/cm^2/surface radiance) is shown and quantified at day 21 in *Right*. Red circles 1 and 2 show the tibiae of experimental animals displayed in *B* and *C*. (*B*) Tibiae metastases were imaged by μCT and reconstructed using maximum-intensity projection (MIP) and volume rendered (VR-3D) 3D techniques. Yellow arrows indicate tumor lesions. (Scale bars of μCT images: 500 μm and 50 μm [enlarged images].) (*C*) RFP signal representing tibial bone metastasis of LNCaP-Trop2-OV cells (yellow arrowheads). Tibiae and livers were also imaged with dark-field (DF) application in *C*, *D*, *G*, and *H*. The percentage of mice with bone metastasis is shown in the *Right*. IHC of bone metastases demonstrates expression of human Trop2. B.M., bone marrow. (Scale bar: 2 mm.) (*D*) RFP signal of the liver surface for LNCaP-RFP and RFP-labeled LNCaP-Trop2-OV. IHC for human Trop2 is shown in the Middle. (Scale bars: 1 mm, low power, and 250 μm, high power images.) Number and size of liver metastases based on counting of the RFP foci using ImageJ are shown at *Right*. (*E*) Bioluminescence activity 21 d after intracardiac injection of 1×10^5 luciferase-labeled DU145-RFP, DU145-Trop2-KO, and DU145-Trop2-OV cells in male NSG mice ($n = 5$ to 6). Red circles 3, 4, and 5 indicate the tibiae of the same experimental animals displayed in *F* and *G*. BLI is shown graphically on the *Right*. (*F*) Volume rendered μCT images of tibial lesions (indicated by the yellow arrows) of the DU145-derived cell lines. (Scale bars of μCT images: 500 μm and 50 μm [enlarged images].) (*G*) Fluorescence microscopy of harvested hind limbs for RFP demonstrating bone metastases indicated by the yellow arrowheads. (Scale bars: 2 mm.) The percentage of mice with bone metastasis is quantified in the *Right*. (*H*) Liver lesions in the DU145-derived cell lines displayed in *D* imaged for surface RFP expression, and sliced FFPE tissues stained for hTrop2 IHC. Number of metastatic foci and size of foci quantified in *Right*. Error bars depict SEM. (Scale bars: 1 mm, low power, and 250 μm, high power images.) *$P <$ 0.05, **$P < 0.01$, ***$P < 0.005$; n.s., not significant.

RFP/DAPI imaging of longitudinally sectioned tibias and IHC for human Trop2 confirmed the presence of LNCaP-Trop2-OV cells (Fig. 4 *C*, *Lower*). Additionally, LNCaP-Trop2-OV cells were found in the lung and liver in 100% (9 of 9) of mice, compared to LNCaP-RFP, where metastases were found in the lung of 27% of mice (3 of 11) and liver in 18% (2 of 11), respectively (*SI Appendix*, Fig. S6*A*). Furthermore, the number and size of liver metastatic nodules were significantly greater in the LNCaP-Trop2-OV injected mice compared to the LNCaP-RFP controls (Fig. 4*D*).

In parallel experiments, to measure prostate cancer colonization, we performed intracardiac injection of luciferase expressing DU145-RFP, DU145-Trop2-OV, and DU145-Trop2-KO cells. BLI at day 21 postinjection revealed that DU145-Trop2-OV injected mice had significantly higher whole-body bioluminescence compared to DU145-Trop2-KO and DU145-RFP cells (Fig. 4*E*). Although total body bioluminescence was similar for DU145-Trop2-KO and DU145-RFP controls, there were no detectable bone metastases in the DU145-Trop2-KO injected mice, compared to 40% of DU145-RFP controls (Fig. 4 *E–G* and *SI Appendix*, Fig. S6 *B*, *Left*). We confirmed the presence of tibial bone metastases using μCT (Fig. 4*F*) and PET/CT imaging (*SI Appendix*, Fig. S6 *B*, *Right*). Similar to our observations with the LNCaP cell models, DU145 bone colonization was significantly increased by Trop2 expression (Fig. 4 *F* and *G* and *SI Appendix*, Fig. S6*B*). Bone metastases were found in 83% (five of six) of mice bearing DU145-Trop2-OV, compared to DU145-RFP control mice (40% or two of five), and 0% of DU145-Trop2-KO injected mice (Fig. 4*G* and *SI Appendix*, Fig. S6*B*). Similarly, modulation of Trop2 had a significant impact on liver colonization, with DU145-Trop2-OV mice displaying increased tumor nodule number and size when compared to the RFP controls (Fig. 4*H*). Although we did not observe significant differences in tumor nodule number between DU145-Trop2-KO and DU145-RFP controls, DU145-Trop2-KO liver metastases were significantly smaller than those observed in DU145-RFP and DU145-Trop2-OV injected animals (Fig. 4*H*).

To confirm the role of Trop2 in prostate cancer metastasis, we assessed rates of metastasis in an s.c. xenograft tumor model (*SI Appendix*, Fig. S7 *A*, *Left Scheme*). In this model, primary tumors (LNCaP-RFP, LNCaP-Trop2-OV, DU145-RFP, and DU145-Trop2-OV) expressing luciferase were resected after they reached volumes of 400 mm^3, and spontaneous metastasis was evaluated after 3 to 4 wk by BLI (*SI Appendix*, Fig. S7 *A*, *Left Scheme*). LNCaP-RFP cells showed no metastases whereas LNCaP-Trop2-OV cells metastasized to the lung (four of six), liver (five of six), and kidney (two of six) 4 wk after resection of the primary tumors (*SI Appendix*, Fig. S7 *A–D*). Similar results were observed using DU145-RFP and DU145-Trop2-OV luciferase-expressing cells. While DU145-RFP control cells did metastasize, overexpression of Trop2 led to a significant increase in the incidence of metastasis to the liver, kidney, and lymph nodes 3 wk after resection of the s.c. primary tumors (*SI Appendix*, Fig. S7 *E–H*). Collectively, our results demonstrate that Trop2 is sufficient to promote prostate cancer colonization and metastasis.

Trop2 Drives Neuroendocrine Phenotype and High Levels of PARP1. To further investigate the role of Trop2 in prostate cancer, we performed proteomic analyses of tumor samples from LNCaP-RFP and LNCaP-Trop2-OV xenografts. Two tumors were analyzed per experimental group, and each tumor was analyzed in triplicate (Fig. 5*A*). Poly(ADP-Ribose) polymerase 1 (PARP1) was the most significant protein, with increased levels (>1,000-fold) in LNCaP-Trop2-OV tumors compared to LNCaP-RFP (Fig. 5 *A* and *B*). Functional enrichment analysis of the 121 up-regulated proteins and 125 down-regulated proteins in LNCaP-Trop2-OV tumors using STRING (https://string-db.org/) (21) was performed (*SI Appendix*, Fig. S8*A*). The most highly enriched protein association network for Trop2 up-regulated proteins in LNCaP-Trop2-OV tumors was "DNA replication and chromosome organization," with PARP1 at the central node of the cluster (Fig. 5*C*). Interestingly, 48% (62 of 125) of the decreased proteins belonged to a set of androgen responsive genes (ARGs) described previously (22), including KLK3 (PSA), an androgen regulated gene used clinically in prostate cancer management (Fig. 5 *A* and *B* and *SI Appendix*, Fig. S8*B*). Consistent with the observed down-regulation of AR-responsive genes, LNCaP-Trop2-OV cells and xenografts showed significantly decreased AR and PSA expression when compared to LNCaP-RFP (Fig. 5 *D–F*). Prostate-specific membrane antigen (PSMA) was found as the most significantly decreased protein in LNCaP-Trop2-OV tumors (Fig. 5 *A* and *B*), and PSMA is known to be suppressed in NEPC (23). We further investigated the effect of Trop2 on PARP1 and AR levels. Complete loss of TROP2 led to a significant reduction of PARP1 levels (*SI Appendix*, Fig. S9*A*) while overexpression of Trop2 resulted in an increase in PARP1 and loss of AR (Fig. 5 *D–F* and *SI Appendix*, Fig. S9*B*). To investigate the kinetics of AR down-regulation and PARP1 up-regulation driven by Trop2, we utilized a doxycycline-inducible overexpression system (*SI Appendix*, Fig. S10 *A* and *B*). PARP1 up-regulation was detectable as early as 72 h post-Trop2 induction (*SI Appendix*, Fig. S10*A*) while AR down-regulation was observed 6 d post-Trop2 induction (*SI Appendix*, Fig. S10*B*). Further gene expression analysis confirmed AR down-regulation and PARP1 up-regulation in Trop2-overexpressing cells (*SI Appendix*, Fig. S10*C*).

PARP1 up-regulation and AR loss are commonly observed in NEPC, and we found that protein levels of neuroendocrine markers (CD56, synaptophysin [SYP], and chromogranin-A [CHGA]) were increased in LNCaP-Trop2-OV cells and tumors (Fig. 5 *D–F* and *SI Appendix*, Fig. S9*B*). We also found high expression of lineage plasticity-associated proteins Sox2, Ezh2, c-Myc, and Oct3/4 in LNCaP-Trop2-OV cells and tumors when compared to LNCaP-RFP (Fig. 5*F* and *SI Appendix*, Fig. S9*B*). Sox2 and Ezh2 were previously reported to promote resistance to anti-androgens and lineage plasticity during the emergence of NEPC accompanied by loss of luminal lineage markers and acquisition of basal-cell markers (24–26). Consistent with previous reports, overexpression of Trop2 led to a significant down-regulation of luminal markers (AR and CK8) and up-regulation of basal cell markers (p63) (*SI Appendix*, Fig. S9*B*). While down-regulation of Trop2 in Trop2-overexpressing LNCaP cells was not sufficient to restore AR expression and had marginal effect on PARP1 levels, knockdown of Trop2 led to a reduction of Ezh2, Sox2, and neuroendocrine markers (SYP and CD56) (*SI Appendix*, Fig. S10*D*). Those results suggest that complete loss of Trop2 might be required to restore the endogenous levels of AR and PARP1 in LNCaP-Trop2-OV cells which do not endogenously express Trop2.

We further investigated the effect of Trop2 on PARP1 and neuroendocrine phenotype across multiple prostate cancer cell lines (*SI Appendix*, Fig. S11*A*). Overexpression of Trop2 led to a significant increase of PARP1 in all cell lines tested except 22Rv1, most likely due to the high baseline endogenous levels of PARP1 in these cells (*SI Appendix*, Fig. S11*A*). Overexpression of Trop2 was associated with a significant down-regulation of AR in LNCaP, and AR and AR-V7 splice variant in 22Rv1, but not in VCaP prostate cancer cells. Trop2 overexpression induced the expression of the neuroendocrine marker CD56 in some prostate cancer cell lines but not in others (*SI Appendix*, Fig. S11*A*). Considering all tested prostate cancer cell lines have distinct known genetic alterations (summarized in *SI Appendix*, Fig. S11*B*), our results suggest that the role of Trop2 in promoting neuroendocrine phenotype is potentially dependent on the genetic context.

PARP1 is an enzyme that regulates DNA replication by controlling the replication fork, DNA repair, transcription, and chromatin remodeling (27–29) and is highly expressed in small cell lung cancer (SCLC), a neuroendocrine subtype of lung cancer, and NEPC (30, 31). Consistent with the significant changes in cell growth and PARP1 levels upon Trop2 modulation, we observed a significant increase in DNA synthesis measured by BrdU incorporation and other proteins involved in DNA replication upon Trop2 overexpression (*SI Appendix*, Fig. S12). In addition to PARP1, we also observed a significant up-regulation of proteins involved in DNA repair in Trop2-OV tumors (*SI Appendix*, Fig. S13*A*). We further measured the efficiency of DNA repair upon DNA damage induced by hydrogen peroxide (H_2O_2) using phospho-γH2A.X intensity as a

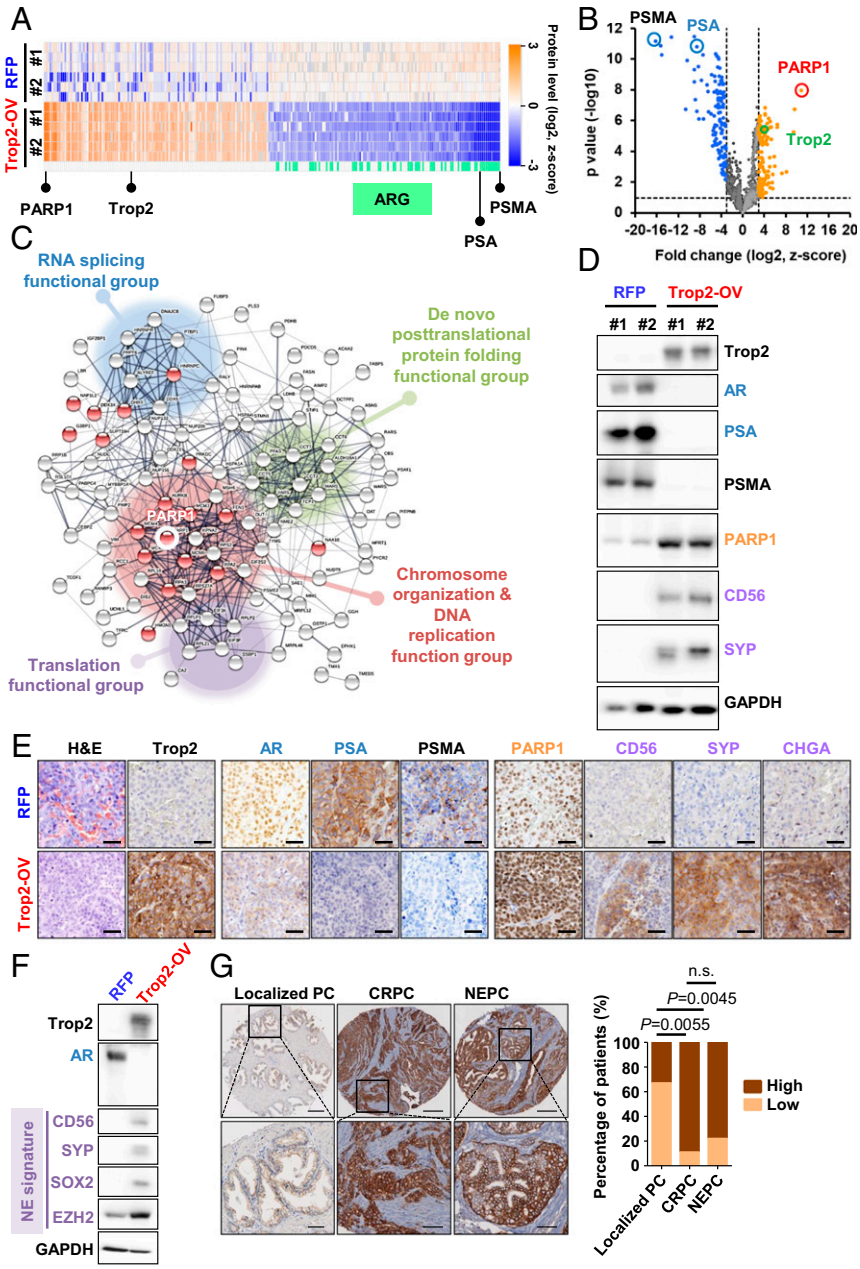

Fig. 5. Tumors driven by Trop2 exhibit neuroendocrine features and high levels of PARP1. (*A*) Heat map displaying fold change of 121 up-regulated and 125 down-regulated proteins in two independent LNCaP-Trop2-OV tumor xenografts and LNCaP-RFP control tumors assessed by mass spectrometry-based shotgun proteomics. In LNCaP-Trop2-OV tumors, PARP1 is the most highly up-regulated protein, and the AR target PSA is significantly repressed. Previously identified androgen responsive genes (ARG) are labeled in green. (*B*) Volcano plot of the Trop2-regulated candidates with the dotted lines representing P value < 0.01 and fold change > eightfold. (*C*) Functional protein association networks for Trop2 up-regulated proteins (n = 121) were analyzed using STRING (https://string-db.org/). The red node indicates a cluster of proteins related to chromosome organization (n = 18). Four major functional groups (clusters) including RNA splicing (blue), translation (purple), protein folding (green), DNA replication, and chromosome organization (red) are indicated. Line thickness indicates the strength of data support of correlation between each node. (*D*) Western blot for Trop2, AR, PSA (AR and AR targets in blue), PSMA (in black), PARP1 (in orange), CD56, SYP (neuroendocrine markers in purple), and glyceraldehyde-3-phosphate dehydrogenase (GAPDH) (loading control) in the LNCaP-RFP and LNCaP-Trop2-OV tumor lysates used for proteomic analysis. (*E*) H&E and IHC staining for Trop2, AR, PSA, PSMA, PARP1, CD56, SYP, and CHGA in LNCaP-RFP and LNCaP-Trop2-OV tumors. (Scale bars: 50 μm.) (*F*) Western blot for AR, CD56, SYP, SOX2, EZH2, and GAPDH in LNCaP-RFP and LNCaP-Trop2-OV cells. (*G*) Staining intensity of Trop2 in localized prostate cancer (localized PC) (n = 12), CRPC (n = 9), and NEPC (n = 23). (Scale bars: 200 μm, low power; and 50 μm, high power.) Distribution of Trop2 staining intensity of prostate tumor samples is shown in the *Right*. The statistical significance of the differences between localized PC, CRPC, and NEPC proportions was calculated by the normal distribution (0,1) of the z-score.

marker of double strand breaks. Surprisingly, overexpression of Trop2 led to a significant accumulation of phospho-γH2A.X upon DNA damage and more damage induced by H_2O_2 (*SI Appendix*, Fig. S13 *B* and *C*). Together, these results suggest that Trop2 overexpression increases DNA replication, resulting in a greater accumulation of DNA damage, and, even though PARP1 and other DNA repair proteins are up-regulated, their levels are still not sufficient to repair the increased DNA damage.

We further evaluated Trop2 protein expression in clinical samples using tissue microarrays (TMAs) of localized prostate cancer, CRPC, and NEPC. High expression of Trop2 protein was found in 89% of CRPC and 78% of NEPC, compared to 33% of localized prostate cancer samples (Fig. 5*G*), and 92% of patients with high Trop2 also had high levels of PARP1 (*SI Appendix*, Fig. S14).

Consistent with the significant down-regulation of AR in Trop2-driven NEPC, cells overexpressing Trop2 were resistant to androgen depletion and the second-generation antiandrogen, enzalutamide (ENZ) (Fig. 6). We compared cell proliferation rates of LNCaP-Trop2-OV to LNCaP-RFP controls grown in medium supplemented with charcoal stripped fetal bovine serum (FBS) (csFBS-androgen depleted) or supplemented with FBS (androgen replete) or upon treatment with ENZ (Fig. 6 *A* and *B*). LNCaP-Trop2-OV cells displayed an androgen-independent cell proliferation, with comparable proliferation rates in androgen-depleted and replete media or vehicle and ENZ treatment while LNCaP-RFP cells were either unable to grow under androgen-depleted conditions or their growth was significantly delayed by ENZ (Fig. 6 *A* and *B*). These findings were further confirmed utilizing a tumorsphere growth assay in csFBS or FBS supplemented medium (Fig. 6*C*). Small tumorspheres could be detected from LNCaP-RFP control cells only after 21 d in FBS, and almost no tumorspheres were observed for LNCaP-RFP cells grown in androgen-depleted conditions. On the other hand, LNCaP-Trop2-OV cells showed significantly higher tumorsphere formation at day 15 in csFBS and FBS, measured by tumorsphere number and size, when compared to LNCaP-RFP cells (Fig. 6*C*). Consistent with these results, LNCaP-Trop2-OV cells were also resistant to ENZ measured by colony formation (*SI Appendix*, Fig. S15*A*).

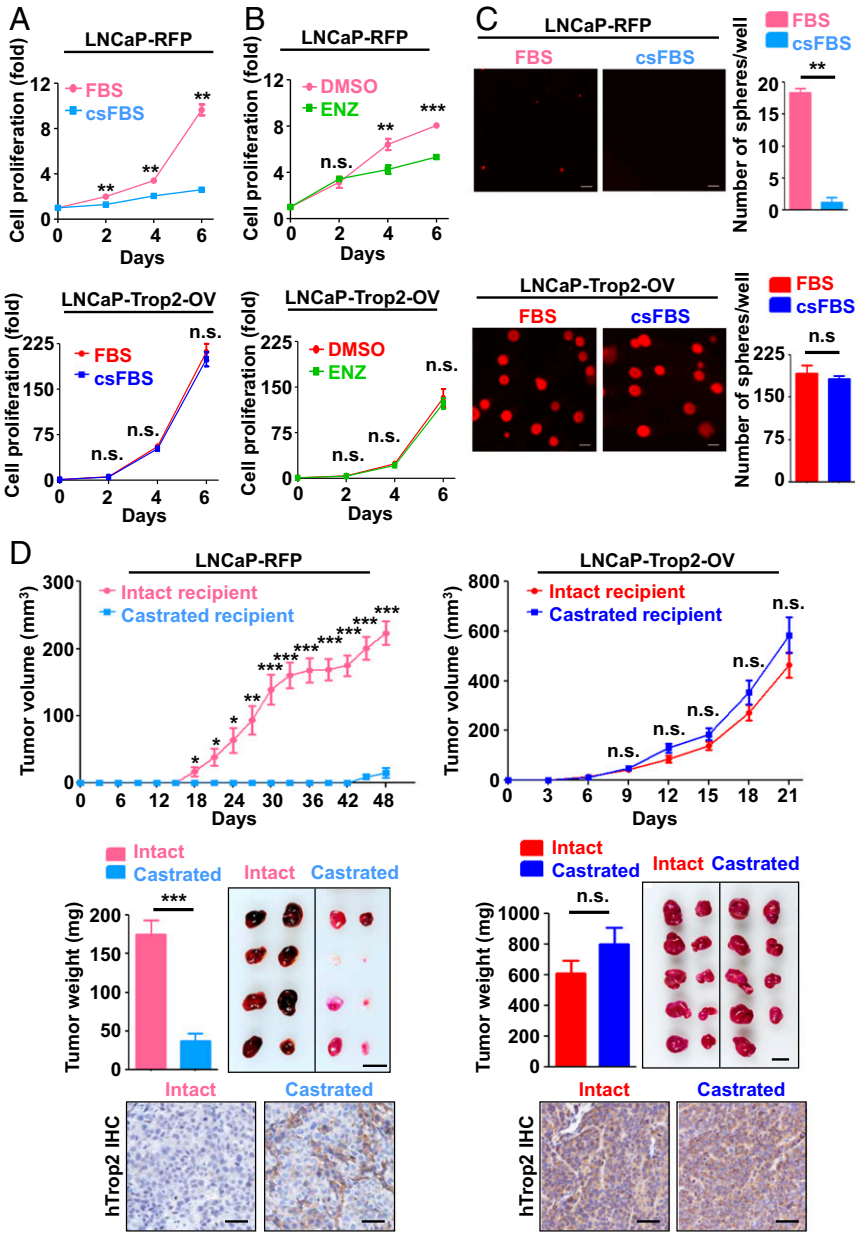

Fig. 6. Trop2-overexpressing cells and tumors are insensitive to androgen ablation in vitro and in vivo. (*A*) Proliferation of LNCaP-RFP and LNCaP-Trop2-OV grown in RPMI (RPMI 1640 medium) supplemented with androgen replete FBS or charcoal stripped FBS (csFBS), which is depleted of androgens. The medium was replaced every 2 d. Cell proliferation is plotted as percentage increase (fold-change) compared to day 0. Bars represent SD. One of three independent experiments is shown. (*B*) Cell proliferation of LNCaP-RFP and LNCaP-Trop2-OV upon treatment with vehicle, dimethyl sulfoxide (DMSO), or enzalutamide (5 μM) is plotted as fold-change compared to day 0. Error bars = SD. (*C*) Tumorsphere assay of LNCaP-RFP and LNCaP-Trop2-OV-RFP cells grown in either 10% FBS or 10% csFBS containing RPMI. The number of tumorspheres per well was counted at day 21 (LNCaP-RFP) and day 15 (LNCaP-Trop2-OV) based on RFP signal using ImageJ. (Scale bars: 300 μm.) The experiment was performed in triplicate, and representative images are shown. Error bars = SD. (*D*) Growth of xenografts of LNCaP-RFP or LNCaP-Trop2-OV in intact or castrated recipient male NSG mice (n = 8 to 10 tumors per experimental group). Tumor weight and harvested tumors are shown *Below* (Scale bar: 1 cm.). Human Trop2 expression by IHC is shown at the *Bottom* (Scale bars: 50 μm.). Error bars represent SEM. *$P < 0.05$, **$P < 0.01$, ***$P < 0.005$; n.s., not significant; as determined by Student's t test at each measurement point.

In both intact and surgically castrated mice, LNCaP-Trop2-OV tumors grew much more rapidly, with detectable tumors as early as 6 d postimplantation, while LNCaP-RFP became palpable only 18 d postimplantation in intact mice and after 45 d in castrated mice (Fig. 6*D*). LNCaP-Trop2-OV tumors grew rapidly and exhibited castration resistance. Interestingly, the LNCaP-RFP tumors that grew in the castrated mice after 45 d showed spontaneously induced expression of Trop2 by IHC (Fig. 6*D*), further suggesting an important role of Trop2 in aggressive prostate cancer. Finally, we implanted LNCaP-Trop2-OV and LNCaP-RFP tumors in intact mice until the average tumor volume reached 200 mm^3 and then castrated the animals (*SI Appendix*, Fig. S15 *B* and *C*). Once again, LNCaP-Trop2-OV xenografts continued to grow independent of castration while LNCaP-RFP tumors rapidly regressed after castration (*SI Appendix*, Fig. S15 *B* and *C*). These results demonstrate that cells overexpressing Trop2 were insensitive to androgen depletion.

Trop2-Driven NEPC Is Sensitive to PARP1 Inhibition. PARP1 was markedly up-regulated in LNCaP-Trop2-OV cells in vitro and was enzymatically active, as demonstrated by increased Poly(ADP-ribosyl)ation (PARylation) of cellular proteins detected using a poly ADP ribose (anti-PAR) antibody (Fig. 7 *A* and *B*). PARylation could be inhibited by treatment with talazoparib or olaparib (Fig. 7*B*). Olaparib is a PARP1 inhibitor currently approved for the treatment of BRCA mutated ovarian, fallopian tube, peritoneal, and breast cancers. Similarly, talazoparib is a PARP1 inhibitor recently approved by the FDA to target BRCA mutated breast cancer and exhibits 100-fold higher potency compared to olaparib (32). Both talazoparib and olaparib decreased colony formation of LNCaP-Trop2-OV cells in a dose-dependent manner (Fig. 7*C*). Furthermore, PARP inhibition reversed the DNA condensation pattern and histone methylation landscape (chromatin remodeling) induced by Trop2 overexpression (*SI Appendix*, Fig. S16 *A* and *B*). Small nuclear size and a speckled heterochromatin aggregation pattern are two histopathologic features associated with the SCLC subtype, and the latter feature is associated with neuroendocrine differentiation (33). Olaparib and talazoparib reversed the Trop2-mediated decrease in nuclear size and histone methylation (H3K27me3) and led to an increase in heterogeneous chromatin pattern (*SI Appendix*, Fig. S16). These results suggest that DNA

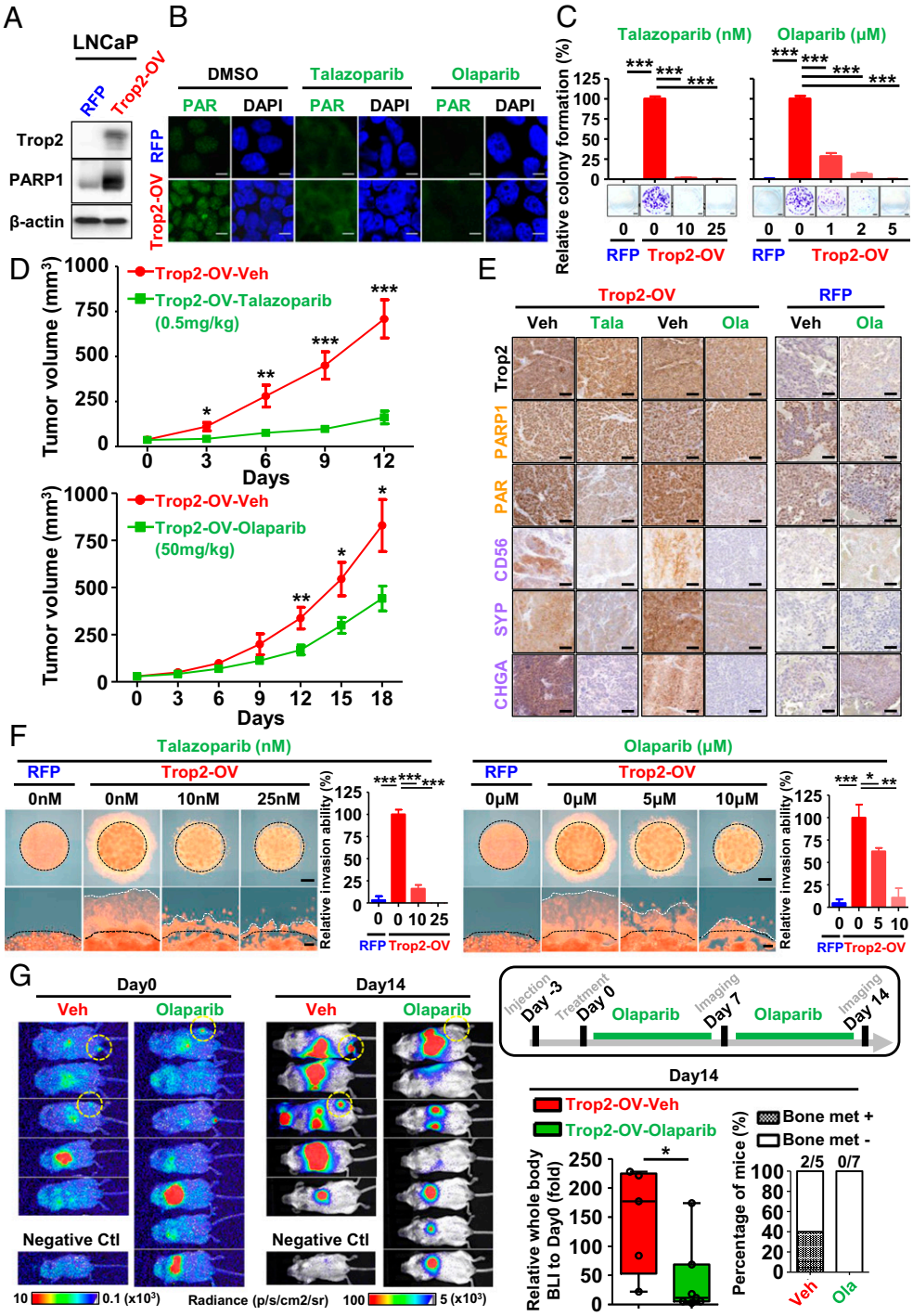

Fig. 7. Targeting PARP1 enzyme activity in Trop2-driven NEPC suppresses tumor growth, bone metastasis, and reverses Trop2-induced NEPC phenotype. (*A*) Western blot of Trop2 and PARP1 proteins in LNCaP-RFP and LNCaP-Trop2-OV. (*B*) Immunocytochemistry and confocal imaging for Trop2, and PARP1 enzyme activity (PARylation) in paraformaldehyde-fixed LNCaP-RFP and LNCaP-Trop2-OV cells treated with DMSO control, talazoparib (10 nM) or olaparib (10 μM) for 3 d. (Scale bars: 10 μm.) (*C*) Colony formation assays of LNCaP-RFP or LNCaP-Trop2-OV cells treated with talazoparib (0–25 nM) or olaparib (0–5 μM). At day 9, the colonies were fixed and stained with crystal violet, and the percentage of colony area per well is plotted as percent colony formation relative to the Trop2-OV treated with vehicle. (*D*) Growth of LNCaP-Trop2-OV s.c. xenografts treated daily with talazoparib (0.5 mg/kg) or olaparib (50 mg/kg), injected i.p. (tumor $n = 7$ to 11 per experimental group). (*E*) IHC staining for Trop2, PARP1, and PARP1 enzyme activity (PARylation), and three neuroendocrine markers (CD56, SYP, and CHGA) in LNCaP-Trop2-OV tumor xenografts treated with vehicle (veh), talazoparib (Tala) or olaparib (Ola) or LNCaP-RFP control with vehicle or olaparib. (Scale bars: 50 μm.) (*F*) Matrigel drop invasion assays of LNCaP-RFP or LNCaP-Trop2-OV cells treated with talazoparib or olaparib. Representative images of invading edge of the whole Matrigel drop (*Upper*) and enlarged image (*Lower*) are shown. The percentage of relative invading area per drop is shown in the *Right Graph*. (Scale bars: 1 mm [*Upper*] and 200 μm [*Lower*].) (*G*) Olaparib decreases metastasis of LNCaP-Trop2-OV cells in an intracardiac injection model. Olaparib (50 mg/kg) or vehicle control began 3 d after intracardiac injection with imaging at 7 and 14 d (see *Insert* of study design). BLI of mice at day 0 and day 14 of control (Ctl) and olaparib-treated animals is shown at *Left*, and whole body quantified BLI is shown at the *Bottom Right*. Percentage of mice with tibial bone metastasis in control and olaparib-treated mice is shown at *Bottom Right*. Error bars represent SD, and in vivo panels error bar = SEM. **P* value < 0.05, ***P* value < 0.01, and ****P* value < 0.005, assessed by Student's *t* test.

condensation and decrease in histone methylation in Trop2-overexpressing cells are mediated through PARP1. Previous studies across diverse cancer types suggest that a heterogeneous chromatin pattern is prognostic in colon, ovarian, endometrial, and prostate cancer (34).

As Trop2-expressing NEPC displays increased PARP1 expression and activity, we next evaluated whether Trop2-expressing NEPC is sensitive to PARP inhibitors in vivo. LNCaP-Trop2-OV xenografts were treated with talazoparib (0.5 mg/kg intraperitoneally [i.p.] daily) or olaparib (50 mg/kg i.p. daily) when the implanted tumor volume reached an average of 25 to 50 mm^3 (Fig. 7*D*). LNCaP-Trop2-OV tumors were highly sensitive to talazoparib when compared to tumors in vehicle-treated animals (Fig. 7*D* and *SI Appendix*, Fig. S17*A*). Similarly, olaparib significantly decreased LNCaP-Trop2-OV tumor growth while it had no significant effect on LNCaP-RFP controls (Fig. 7*D* and *SI Appendix*, S17 *B* and *C*). IHC demonstrated that LNCaP-Trop2-OV xenografts expressed Trop2 and PARP1 while treated xenografts showed decreased PARylation and significantly decreased expression of neuroendocrine markers CD56, SYP, and CHGA (Fig. 7*E*).

To assess the effects of PARP inhibition on Trop2-induced cancer cell invasion, we treated LNCaP-RFP or LNCaP-Trop2-OV cells with talazoparib (0, 10, and 25 nM) or olaparib (0, 5, and 10 μM) using the three-dimensional (3D) Matrigel drop invasion model described above. PARP inhibition significantly decreased invasion and migration outside of the Matrigel drop in a dose-dependent fashion (Fig. 7*F*). To further evaluate the role of PARP1 in Trop2-induced metastatic colonization, we tested the effects of PARP inhibitors in an intracardiac injection mouse model. Mice were matched based on similar bioluminescent intensity at day 0 and then randomized to receive either olaparib (50 mg/kg i.p. daily) or vehicle control for 14 d. Whole body bioluminescent signal recorded at days 0 and 14 demonstrated that olaparib reduced total metastatic burden, including bone metastasis to the hind limbs (Fig. 7*G*, bone metastases indicated by yellow circles). Therefore, PARP1 activity is essential for Trop2-driven tumor growth, metastasis, and NEPC phenotype.

Discussion

NEPC exhibits small cell carcinoma or neuroendocrine features characterized by distinct histopathology, aggressive phenotype, down-regulation of AR, and expression of neuroendocrine markers (6–9, 35, 36). Identifying new drivers of NEPC is imperative for understanding the mechanisms underlying NEPC development and for defining new therapeutic strategies. In this study, we identified Trop2 as a driver for neuroendocrine phenotype. Elevated levels of Trop2 are associated with biochemical recurrence of localized prostate cancer, and Trop2 is highly expressed in CRPC and NEPC. Additionally, overexpression of Trop2 induced lineage plasticity characterized by loss of luminal cell markers, gain of basal cell markers, and NEPC phenotype. Our findings are consistent with previous reports demonstrating that androgen ablation enriches for prostate basal-like cells with high Trop2 (16). Consistent with the elevated levels of Trop2 in localized prostate cancer, overexpression of Trop2 alone in normal epithelial cells was shown to drive highly proliferative neoplastic lesions (15). Here, we find that, while Trop2 consistently enhances cell growth across different prostate cancer cell lines, Trop2 leads to a significant down-regulation of AR in LNCaP and 22Rv1 but not in VCaP prostate cancer cells, and it is able to induce the neuroendocrine marker CD56 in some prostate cancer cell lines but not in others. These findings suggest that Trop2 may play a context-dependent role in distinct stages of the disease. Indeed, all tested prostate cancer cell lines have distinct genetic alterations, and it has been previously reported that the NEPC phenotype is driven by a combination of alterations (24, 25, 37–39). Future studies will be conducted to delineate the genetic or epigenetic alterations enabling different roles of Trop2 in distinct stages of prostate cancer.

Trop2-driven NEPC displayed low expression of AR and induction of neuroendocrine markers similar to that observed in other CRPC/NEPC models (37, 38). Trop2-driven NEPC also expresses high levels of Sox2 and Ezh2 (Fig. 5*F*), previously shown to promote antiandrogen resistance and lineage plasticity during the emergence of NEPC (24–26). Consistent with the lineage plasticity phenotype driven by Sox2 and Ezh2, overexpression of Trop2 led to a significant down-regulation of luminal markers (AR and CK8), up-regulation of basal cell markers (p63), and up-regulation of Sox2 and Ezh2 (Fig. 5*F* and *SI Appendix*, Fig. S9*B*). Due to the significant decrease in histone methylation (H3K27me3) observed upon overexpression of Trop2 and its reversal upon treatment with PARP inhibitors, our study suggests that the role of Ezh2 in the context of Trop2 overexpression is independent of its methyltransferase activity. We speculate that Trop2 may induce lineage plasticity accompanied by a loss of luminal identity and down-regulation of luminal markers including AR, in a context-dependent manner.

Metastatic prostate cancer is invariably lethal. Bone is the most common metastatic site while liver metastasis is commonly associated with NEPC and poor survival (20, 40). Previous studies have demonstrated that Trop2 fosters cancer cell migration and invasion in multiple cancer types (18, 19, 41). Consistent with these studies, we found that elevated expression of Trop2 significantly enhanced migration and invasion while loss of Trop2 inhibited both. Trop2 was particularly effective at causing bone and liver colonization in an intracardiac injection model and lung, liver, and lymph node metastasis in a spontaneous metastasis model, mirroring the human disease, and substantiating a significant functional role for Trop2 in prostate cancer progression and metastasis. Importantly, our findings suggest that targeting the Trop2 pathway may represent a novel therapeutic strategy for metastatic prostate cancer.

PARP1 as well as other proteins involved in DNA replication and chromosome organization were unexpectedly up-regulated in response to Trop2 overexpression. PARP1 has many known functions, including DNA repair, DNA replication, cell death, chromatin remodeling, inflammation, and transcriptional regulation (42). Consistent with the role of PARP1 in DNA replication, we observed a significant increase in DNA synthesis. Previous studies demonstrated that PARP1 is necessary for AR-driven gene expression (29). In addition, AR signaling is required to activate the DNA repair pathway, further suggesting that targeting both AR and PARP pathways could be an effective approach to treat advanced prostate cancer (43). In our study, Trop2-driven NEPC displays high levels of PARP1 and a significant down-regulation of AR and AR downstream targets, suggesting an AR-independent role of PARP1 during transdifferentiation to NEPC in the context of Trop2 overexpression. Elevated PARP1 is associated with the neuroendocrine phenotype of SCLC and other neuroendocrine cancers (30). Due to the role of PARP1 in DNA repair, the PARP inhibitor, olaparib, is currently used for the treatment of BRCA mutated ovarian, fallopian tube, peritoneal, and breast cancers. More recently, the FDA approved talazoparib for patients with HER2-negative locally advanced or metastatic breast cancer with germline BRCA mutations. In prostate cancer, mutations in BRCA1, BRCA2, and ATM genes are observed in roughly 20% of advanced prostate cancer (44). Clinical responses have been observed utilizing PARP inhibitors in CRPC with these mutations (45). Trop2-driven prostate cancer xenografts are sensitive to PARP inhibition, in concordance with findings in SCLC where PARP inhibition is effective in tumors with abundant PARP1 protein expression (30). Our study demonstrates a link between Trop2, PARP1, and neuroendocrine transdifferentiation and suggests that there could be additional subsets of NEPC with elevated Trop2 expression that are sensitive to PARP inhibitors. Since high expression of Trop2 is known to occur in many epithelial malignancies, PARP inhibitors could be effective if a similar linkage between Trop2 and PARP is observed.

The molecular mechanisms through which Trop2 regulates PARP1 are still to be delineated. It has been previously reported that Trop2 is cleaved, leading to translocation of the intracellular domain to the nucleus where Trop2 may serve as a cotranscriptional factor and regulate c-Myc expression (15). Interestingly, c-Myc is the key transcription factor that directly binds to the PARP1

gene promoter and up-regulates PARP1 expression in induced pluripotent stem cells (iPSCs) (46). Accumulating evidence indicates that PARP1 plays an essential function in maintaining pluripotent status and stem cell reprogramming (27). PARP inhibitors reverse the Trop2-driven NEPC phenotype, suggesting that PARP1 activity contributes to the Trop2-driven neuroendocrine phenotype. Indeed, we observe a significant up-regulation in c-Myc in LNCaP-Trop2-OV cells and tumors and an increase in PARP1 protein and RNA levels. Based on the current lineage plasticity model of NEPC development in prostate cancer, it is possible that Trop2 regulates PARP1 through c-Myc and the Trop2-c-Myc-PARP1 cascade is involved in cell reprogramming and neuroendocrine transdifferentiation of prostate cancer.

In summary, Trop2 is commonly expressed at high levels in metastatic prostate cancer, NEPC, and is prognostic in localized prostate cancer treated surgically. Trop2 induces migration, invasion, tumorsphere formation, and cell proliferation in prostate cancer cells. Furthermore, Trop2 enhances tumorigenicity in prostate cancer xenograft models and increases prostate cancer metastasis. Trop2 drives neuroendocrine transdifferentiation, characterized by loss of luminal markers such as AR, expression of neuroendocrine markers, and high levels of PARP1. Inhibition of PARP1 by talazoparib and olaparib suppresses Trop2-induced nuclear PARylation, reverses the neuroendocrine phenotype, and decreases tumor growth and metastasis in vivo. Collectively, our study demonstrates that Trop2 may represent a prognostic biomarker for disease recurrence, an attractive therapeutic target for late stage metastatic prostate cancer, and could identify a class of cancers sensitive to PARP1 inhibition.

Methods

Detailed methods are available in *SI Appendix, SI Methods*.

Lentiviral Production and Concentration. Lentiviral plasmids FUCRW, FUCRW-Trop2-Flag, pLKO.1-control scramble short hairpin RNA (shRNA) vector, or pLKO.1-Trop2 shRNA were cotransfected using third generation packaging systems, including pMDLg/pRRE, pRSV-Rev, and pMD2.G, into 293T cells using standard calcium phosphate transfection. The media with viral particles were collected for 2 d, filtered using a 0.45-μm filter, and concentrated using ultracentrifugation (25,000 rpm, 2 h). The viral titer was determined through serial dilution of concentrated viruses and infection of 2×10^5 293T cells in six-well plates. The percentage of infected cells (viral titer) was analyzed by the Guava easyCyte Flow Cytometer (EMD Millipore) based on GFP or RFP expression 72 h postinfection.

Human Tissues (Tissue Microarrays). All human samples were deidentified prior to use in this study.

Data Availability Statement. All data and associated protocols are included in the manuscript and available to the readers. Cell lines generated in this study are available upon request.

ACKNOWLEDGMENTS. This work was supported by the Canary Foundation; by NIH/National Cancer Institute K99/R00 Award 4R00CA184397 (to T.S.), R03CA230819 (to T.S.), and U01 CA196387 (to J.D.B.); by Department of Defense Congressionally Directed Medical Research Program (CDMRP) Grants W81XWH1810323 (to T.S.) and W81XWH1810141 (to M.A.R.); and by NIH under Award S10 OD023518-01A1 for the Celigo S Imaging Cytometer (200-BFFL-S). Opinions, interpretation, conclusions, and recommendations are those of the authors and not necessarily endorsed by the US Army.

1. R. L. Siegel, K. D. Miller, A. Jemal, Cancer statistics, 2019. *CA Cancer J. Clin.* **69**, 7–34 (2019).
2. W. P. Harris, E. A. Mostaghel, P. S. Nelson, B. Montgomery, Androgen deprivation therapy: Progress in understanding mechanisms of resistance and optimizing androgen depletion. *Nat. Clin. Pract. Urol.* **6**, 76–85 (2009).
3. H. I. Scher *et al.*; AFFIRM Investigators, Increased survival with enzalutamide in prostate cancer after chemotherapy. *N. Engl. J. Med.* **367**, 1187–1197 (2012).
4. P. J. Vlachostergios, L. Puca, H. Beltran, Emerging variants of castration-resistant prostate cancer. *Curr. Oncol. Rep.* **19**, 32 (2017).
5. R. Nadal, M. Schweizer, O. N. Kryvenko, J. I. Epstein, M. A. Eisenberger, Small cell carcinoma of the prostate. *Nat. Rev. Urol.* **11**, 213–219 (2014).
6. J. I. Epstein *et al.*, Proposed morphologic classification of prostate cancer with neuroendocrine differentiation. *Am. J. Surg. Pathol.* **38**, 756–767 (2014).
7. H. Beltran *et al.*, Molecular characterization of neuroendocrine prostate cancer and identification of new drug targets. *Cancer Discov.* **1**, 487–495 (2011).
8. R. Aggarwal *et al.*, Clinical and genomic characterization of treatment-emergent small-cell neuroendocrine prostate cancer: A multi-institutional prospective study. *J. Clin. Oncol.* **36**, 2492–2503 (2018).
9. E. G. Bluemn *et al.*, Androgen receptor pathway-independent prostate cancer is sustained through FGF signaling. *Cancer Cell* **32**, 474–489.e6 (2017).
10. A. Shvartsur, B. Bonavida, Trop2 and its overexpression in cancers: Regulation and clinical/therapeutic implications. *Genes Cancer* **6**, 84–105 (2015).
11. P. Zeng *et al.*, Impact of TROP2 expression on prognosis in solid tumors: A systematic review and meta-analysis. *Sci. Rep.* **6**, 33658 (2016).
12. D. M. Goldenberg, R. Stein, R. M. Sharkey, The emergence of trophoblast cell-surface antigen 2 (TROP-2) as a novel cancer target. *Oncotarget* **9**, 28989–29006 (2018).
13. D. M. Goldenberg, T. M. Cardillo, S. V. Govindan, E. A. Rossi, R. M. Sharkey, Trop-2 is a novel target for solid cancer therapy with sacituzumab govitecan (IMMU-132), an antibody-drug conjugate (ADC). *Oncotarget* **6**, 22496–22512 (2015).
14. A. Bardia *et al.*, Sacituzumab govitecan-hziy in refractory metastatic triple-negative breast cancer. *N. Engl. J. Med.* **380**, 741–751 (2019).
15. T. Stoyanova *et al.*, Regulated proteolysis of Trop2 drives epithelial hyperplasia and stem cell self-renewal via β-catenin signaling. *Genes Dev.* **26**, 2271–2285 (2012).
16. A. S. Goldstein *et al.*, Trop2 identifies a subpopulation of murine and human prostate basal cells with stem cell characteristics. *Proc. Natl. Acad. Sci. U.S.A.* **105**, 20882–20887 (2008).
17. X. Ju *et al.*, v-Src oncogene induces Trop2 proteolytic activation via cyclin D1. *Cancer Res.* **76**, 6723–6734 (2016).
18. M. Trerotola *et al.*, Trop-2 is up-regulated in invasive prostate cancer and displaces FAK from focal contacts. *Oncotarget* **6**, 14318–14328 (2015).
19. M. Trerotola *et al.*, Trop-2 promotes prostate cancer metastasis by modulating β(1) integrin functions. *Cancer Res.* **73**, 3155–3167 (2013).
20. S. Halabi *et al.*, Meta-analysis evaluating the impact of site of metastasis on overall survival in men with castration-resistant prostate cancer. *J. Clin. Oncol.* **34**, 1652–1659 (2016).
21. D. Szklarczyk *et al.*, The STRING database in 2017: Quality-controlled protein-protein association networks, made broadly accessible. *Nucleic Acids Res.* **45**, D362–D368 (2017).
22. M. Jiang *et al.*, Androgen-responsive gene database: Integrated knowledge on androgen-responsive genes. *Mol. Endocrinol.* **23**, 1927–1933 (2009).
23. M. K. Bakht *et al.*, Neuroendocrine differentiation of prostate cancer leads to PSMA suppression. *Endocr. Relat. Cancer* **26**, 131–146 (2018).
24. P. Mu *et al.*, SOX2 promotes lineage plasticity and antiandrogen resistance in TP53- and RB1-deficient prostate cancer. *Science* **355**, 84–88 (2017).
25. S. Y. Ku *et al.*, Rb1 and Trp53 cooperate to suppress prostate cancer lineage plasticity, metastasis, and antiandrogen resistance. *Science* **355**, 78–83 (2017).
26. J. L. Bishop *et al.*, The master neural transcription factor BRN2 is an androgen receptor-suppressed driver of neuroendocrine differentiation in prostate cancer. *Cancer Discov.* **7**, 54–71 (2017).
27. B. H. Jiang *et al.*, Poly(ADP-Ribose) polymerase 1: Cellular pluripotency, reprogramming, and tumorogenesis. *Int. J. Mol. Sci.* **16**, 15531–15545 (2015).
28. A. Ray Chaudhuri, A. Nussenzweig, The multifaceted roles of PARP1 in DNA repair and chromatin remodelling. *Nat. Rev. Mol. Cell Biol.* **18**, 610–621 (2017).
29. M. J. Schiewer *et al.*, Dual roles of PARP-1 promote cancer growth and progression. *Cancer Discov.* **2**, 1134–1149 (2012).
30. L. A. Byers *et al.*, Proteomic profiling identifies dysregulated pathways in small cell lung cancer and novel therapeutic targets including PARP1. *Cancer Discov.* **2**, 798–811 (2012).
31. W. Zhang *et al.*, Targeting the MYCN-PARP-DNA damage response pathway in neuroendocrine prostate cancer. *Clin. Cancer Res.* **24**, 696–707 (2018).
32. Y. Shen *et al.*, BMN 673, a novel and highly potent PARP1/2 inhibitor for the treatment of human cancers with DNA repair deficiency. *Clin. Cancer Res.* **19**, 5003–5015 (2013).
33. D. Zink, A. H. Fischer, J. A. Nickerson, Nuclear structure in cancer cells. *Nat. Rev. Cancer* **4**, 677–687 (2004).
34. A. Kleppe *et al.*, Chromatin organisation and cancer prognosis: A pan-cancer study. *Lancet Oncol.* **19**, 356–369 (2018).
35. J. L. Yao *et al.*, Small cell carcinoma of the prostate: An immunohistochemical study. *Am. J. Surg. Pathol.* **30**, 705–712 (2006).
36. H. Beltran *et al.*, Divergent clonal evolution of castration-resistant neuroendocrine prostate cancer. *Nat. Med.* **22**, 298–305 (2016).
37. J. K. Lee *et al.*, N-Myc drives neuroendocrine prostate cancer initiated from human prostate epithelial cells. *Cancer Cell* **29**, 536–547 (2016).
38. E. Dardenne *et al.*, N-Myc induces an EZH2-mediated transcriptional program driving neuroendocrine prostate cancer. *Cancer Cell* **30**, 563–577 (2016).
39. J. W. Park *et al.*, Reprogramming normal human epithelial tissues to a common, lethal neuroendocrine cancer lineage. *Science* **362**, 91–95 (2018).
40. H. Beltran *et al.*, The initial detection and partial characterization of circulating tumor cells in neuroendocrine prostate cancer. *Clin. Cancer Res.* **22**, 1510–1519 (2016).
41. H. Guan *et al.*, Trop2 enhances invasion of thyroid cancer by inducing MMP2 through ERK and JNK pathways. *BMC Cancer* **17**, 486 (2017).
42. M. J. Schiewer, K. E. Knudsen, Transcriptional roles of PARP1 in cancer. *Mol. Cancer Res.* **12**, 1069–1080 (2014).
43. M. Asim *et al.*, Synthetic lethality between androgen receptor signalling and the PARP pathway in prostate cancer. *Nat. Commun.* **8**, 374 (2017).
44. D. Robinson *et al.*, Integrative clinical genomics of advanced prostate cancer. *Cell* **161**, 1215–1228 (2015).
45. J. Mateo *et al.*, DNA-repair defects and olaparib in metastatic prostate cancer. *N. Engl. J. Med.* **373**, 1697–1708 (2015).
46. S. H. Chiou *et al.*, Poly(ADP-ribose) polymerase 1 regulates nuclear reprogramming and promotes iPSC generation without c-Myc. *J. Exp. Med.* **210**, 85–98 (2013).